The Astrophysical Journal, 597:986–997, 2003 November 10

CONTINUUM AND CO/HCO$^+$ EMISSION FROM THE DISK AROUND THE T TAURI STAR LkCa 15

Chunhua Qi,[1,2] Jacqueline E. Kessler,[3] David W. Koerner,[4]
Anneila I. Sargent,[5] and Geoffrey A. Blake[1,3]
Received 2003 April 17; accepted 2003 July 11

ABSTRACT

We present Owens Valley Radio Observatory Millimeter Array $\lambda = 3.4$–1.2 mm dust continuum and spectral line observations of the accretion disk encircling the T Tauri star LkCa 15. The 1.2 mm dust continuum emission is resolved and gives a minimum diameter of 190 AU and an inclination angle of $57° \pm 5°$. There is a noticeable but, at present, poorly constrained decrease in the continuum spectral slope with frequency that may result from the coupled processes of grain growth and dust settling. Imaging of the fairly intense emission from the lowest rotational transitions of CO, ^{13}CO, and HCO$^+$ reveals a rotating disk substantially larger than that observed in the dust continuum. Emission extends to $\sim$750 AU and the characteristic radius of the disk is determined to be $\sim$425 AU (HWHM), based on model fits to the CO velocity field. The measured line ratios demonstrate that the emission from these species is optically thick, while that from C^{18}O and H^{13}CO$^+$ is optically thin, or nearly so. The disk mass derived from the CO isotopologues with typical dense cloud abundances is still nearly 2 orders of magnitude less than that inferred from the dust emission, the most probable explanation being extensive molecular depletion in the cold, dense disk midplane. Thus, while CO, HCO$^+$, and their isotopologues are excellent tracers of the disk velocity field, they are not reliable tracers of the disk mass. N_2H^+ $1 \rightarrow 0$ emission has also been detected which, along with HCO$^+$, sets a lower limit to the fractional ionization of 10^{-8} in the near-surface regions of protoplanetary disks. This first detection of N_2H^+ in circumstellar disks has also made possible a determination of the N_2/CO ratio ($\sim$2) that is at least an order of magnitude larger than those in the envelopes of young stellar objects and dense clouds. The large N_2/CO ratio indicates that our observations probe disk layers in which CO is depleted but some N_2 remains in the gas phase. Such differential depletion can lead to large variations in the fractional ionization with height in the outer reaches of circumstellar disks and may help to explain the relative nitrogen deficiency observed in comets.

Subject headings: circumstellar matter — ISM: molecules — planetary systems: protoplanetary disks — radio lines: stars — stars: individual (LkCa 15)

1. INTRODUCTION

LkCa 15, located in the Taurus-Auriga complex at a distance of 140 pc, is rapidly becoming one of the best studied T Tauri stars at millimeter wavelengths. A K5 star with an optical/near-infrared luminosity of $\sim$0.8 $L_\odot$ (Elias 1978; Neuhaeuser et al. 1995; Simon, Dutrey, & Guilloteau 2001), LkCa 15 is well isolated from dark clouds and lacks any detectable reflection nebulosity in *Hubble Space Telescope* (*HST*) WFPC2 images (Krist et al. 1997). Its substantial near- through far-infrared excess is consistent with the presence of a circumstellar disk (Strom et al. 1989) whose mass and radial extent have been determined by recent spectral energy distribution fits and millimeter-wave interferometric observations to be some 0.024 $M_\odot$ and 650 AU, respectively (Chiang et al. 2001; Simon et al. 2001).

Age estimates for LkCa 15 range from 3 Myr (Simon et al. 2001) to 12 Myr (Thi et al. 2001). These timescales are similar to those suggested for the disappearance of small dust grains in the inner regions of circumstellar disks (Skrutskie et al. 1990; Lada 1999; Robberto et al. 1999) and for the differentiation of meteoritic material in the early solar nebula (Alexander, Boss, & Carlson 2001; Amelin et al. 2002).

The large size and mass of the disk, combined with the age of LkCa 15, make this an important system for further study, since it may represent an important transitional phase in which viscous disk spreading and dispersal competes with planetary formation processes. Further, the outer disk can be studied in detail with existing (sub)millimeter-wave telescopes. Single-dish observations have already revealed readily detectable emission from several molecules (van Zadelhoff et al. 2001; Thi et al. 2001), while aperture synthesis imaging has the potential to shed light on the chemical and physical gradients in the disk.

Our initial millimeter-wave observations of LkCa 15 have concentrated on species that are typically abundant in dense molecular clouds. Here we present Owens Valley Radio Observatory (OVRO) Millimeter Array observations of the disk encircling LkCa 15 in dust continuum emission and the lowest rotational transitions of various isotopologues of CO and HCO$^+$. An upper limit to the emission from the H^{13}CO$^+$ ion is noted. N_2H^+ was also observed to constrain the fractional ionization and molecular depletion beyond 100 AU. Due to the limited angular extent of the disk,

[1] Division of Geological and Planetary Sciences, California Institute of Technology 150-21, Pasadena, CA 91125.
[2] Harvard–Smithsonian Center for Astrophysics, 60 Garden Street, MS 42, Cambridge, MA 02138.
[3] Division of Chemistry and Chemical Engineering, California Institute of Technology, Pasadena, CA 91125.
[4] Department of Physics and Astronomy, Northern Arizona University, P.O. Box 6010, Flagstaff, Arizona 86011.
[5] Division of Physics, Mathematics, and Astronomy, California Institute of Technology 103-33, Pasadena, CA 91125.

small-scale gradients were largely smoothed out by the spatial resolution achieved, and the resultant line intensities should be considered as an average over the outer disk. Nevertheless, these interferometric observations suffer from substantially less beam dilution than those with single telescopes, and this, combined with the inherent stability of cross-correlation measurements, provides a powerful means of studying the weak emission from species such as N_2H^+ and $C^{18}O$. While arrays under development will provide substantially improved sensitivity and spatial resolution, observations at the $\lesssim$few arcsecond level form the first and necessary step to understanding depletion and ionization within the disks of T Tauri stars. Future publications will present more detailed analyses of these and other data acquired in an extensive millimeter-wave interferometric spectral line survey of LkCa 15 (Qi, Kessler, & Blake 2003, in preparation; Kessler, Qi, & Blake 2003, in preparation). In what follows, § 2 includes a brief overview of the observations, while in § 3, we discuss the results and the important effects of gas-phase depletion and fractional ionization on the physical and chemical structure of the disk around LkCa 15. A brief summary of our results and the role of future observations may be found in § 4.

2. OBSERVATIONS

All measurements were made between 1997 October and 2000 April using the OVRO Millimeter Array at Big Pine, California. The array consists of six 10.4 m telescopes with an rms surface precision of 35 μm. The pointing accuracy is about 4″, except for brief excursions at sunrise and sunset. Combinations of five array configurations were used to map LkCa 15, with antenna spacings ranging from 20 to 400 m east–west and from 25 to 440 m north–south. Cryogenic SIS receivers on each telescope produced average single sideband system temperatures of 450, 1300, and 1200 K at the frequencies of the ^{13}CO $1 \rightarrow 0$, CO $1 \rightarrow 0$, and CO $2 \rightarrow 1$ lines, respectively. The receivers were tuned for double sideband operation so that both the upper and lower sidebands could be used for molecular line studies.

The receiver IF output is sent over fiber optic transmission lines to a pair of 1 GHz bandwidth analog correlators and a 512 lag digital correlator with four separately configurable modules. Spectral line and continuum measurements are made simultaneously and can be carried out in both the $\lambda = 3$ and 1.3 mm atmospheric windows with a single local oscillator setup. During the ^{13}CO $1 \rightarrow 0$ and HCO^+ $1 \rightarrow 0$ observations of LkCa 15, the digital correlator was configured into two bands of 64×0.125 MHz channels to provide a velocity resolution of 0.17 and 0.21 km s^{-1}, while the CO $2 \rightarrow 1$ measurements were made using 256×0.125 MHz channels for a velocity resolution of 0.16 km s^{-1}.

Calibration of the visibility phases and amplitudes was achieved with observations of the quasars 0528+134 and 0507+179, typically at intervals of 20–30 minutes. Measurements of Uranus, Neptune, 3C 273, and 3C 454.3 provided an absolute scale for the calibration of flux densities. All data were phase- and amplitude-calibrated using the MMA software package, developed specifically for OVRO (Scoville et al. 1993). Continuum and spectral line maps were generated and CLEANed using the NRAO AIPS package. The continuum level is not subtracted in obtaining the line maps because most of the transitions observed here are optically thick, whereas the continuum is optically thin. Uncertainties in the fluxes and source positions are estimated to be 20% and 0.″5, respectively. The synthesized beams vary from 1″ at 1.2 mm to 4″ at 3.4 mm.

2.1. *Continuum Emission*

Figure 1 shows the spectral energy distribution of the continuum emission from LkCa 15. A noticeable but, at present, poorly constrained decrease in the continuum spectral slope with frequency has been found, as discussed further in § 3.1. The dust emission is spatially resolved but only in the highest resolution OVRO 1.2 mm images. The (u, v) plane fits of a two-dimensional Gaussian to the highest quality visibilities yield a deconvolved size of $(1.''35 \pm 0.''12) \times (0.''74 \pm 0.''06)$ at a position angle (P.A.) of $66° \pm 5°$, which corresponds to a minimum size of the dust disk of 189 ± 17 AU. Assuming the disk is circular, the measured ellipticity indicates an inclination angle of $57° \pm 5°$ (0° being the inclination of a face-on disk). This inclination is somewhat larger than the value obtained by Duvert et al. (2000)—34°—but smaller than the value of 66° obtained by Kitamura et al. (2002) with their NMA 2 mm continuum observations, probably because of differences in the synthesized beams. Nevertheless, it is in good agreement with both the OVRO and Plateau de Bure measurements of the disk properties as traced by CO (Simon et al. 2001).

2.2. CO/HCO^+ *Observations*

Figure 2 shows the integrated intensity and intensity-weighted mean velocity maps of the CO $2 \rightarrow 1$ emission toward LkCa 15. As shown in the left panel, the molecular gas emission appears much more extended than the dust. Solid grains no doubt exist at similar radii but are undetectable due to the more rapid fall-off in dust emissivity (Sargent & Beckwith 1987; Lay, Carlstrom, & Hills 1997).

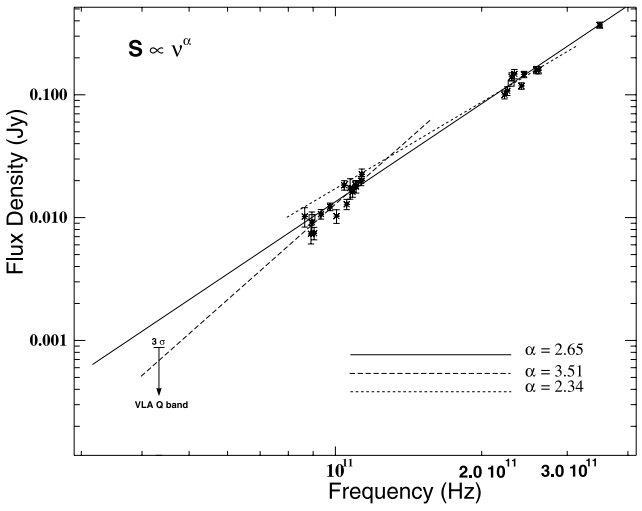

FIG. 1.—Measured millimeter/submillimeter continuum emission fluxes toward LkCa 15. The 850 μm point was acquired with SCUBA, whose image of LkCa 15 is consistent with a point source (G. Sandell 2003, private communication). *Squares*: 3 and 1.3 mm continuum fluxes measured with the Plateau de Bure interferometer (Duvert et al. 2000). *Solid line*: Spectral slope as determined by all of the available data. *Dashed lines*: Individual spectral slope fits to the 3 mm and 1.3 mm data. The 7 mm VLA observations (D. Wilner 2003, private communication) detect no continuum emission to an rms of 0.29 mJy. Even the 3 σ upper limit is inconsistent with an extrapolation of the spectral index derived from the millimeter/submillimeter fluxes.

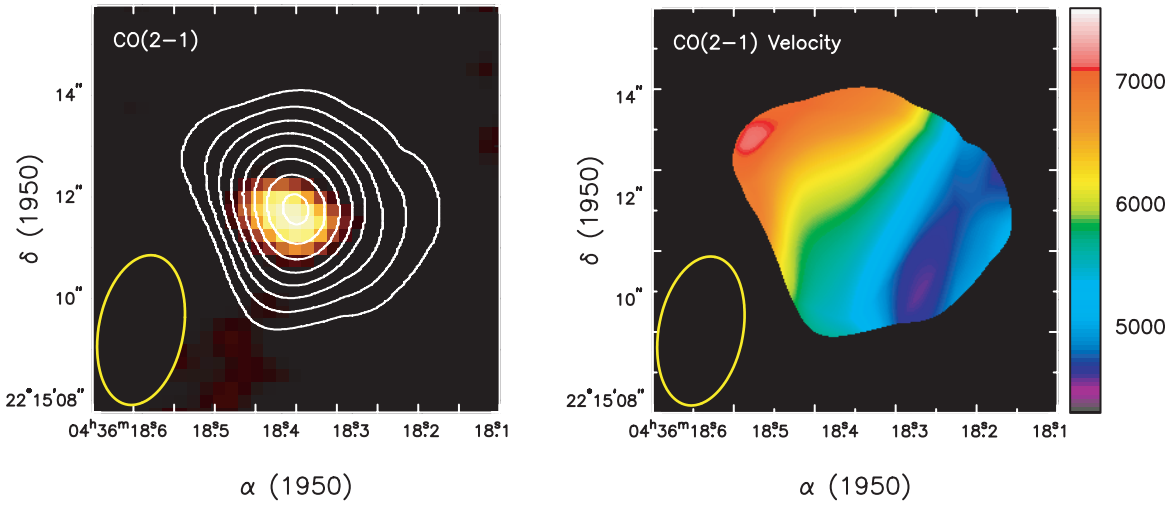

FIG. 2.—CO 2 → 1 emission toward LkCa 15. *Left*: Integrated intensity is shown in contours overlaid on the highest resolution continuum image in gray scale. Contours start at 30% of the peak value of 2.66 Jy km s^{-1} and increase 10% thereafter. The intensity-weighted mean velocity field over the observed emission region is shown at right (v_{LSR} units in m s^{-1}). The synthesized beam is shown at lower left.

Conversely, the molecular emission from the innermost region of the disk ($R < 30$–50 AU) is sufficiently beam-diluted even at 1″–2″ resolution that no direct information on this size scale can be obtained without further improvements in sensitivity and imaging performance. The circumstellar gas emission is an effective tracer of the line-of-sight velocity component of the outer disk via Doppler shifts, as is shown by the intensity-weighted mean gas velocity map in Figure 2 (*right*). Molecular gas southwest (SW) of the star is blueshifted, whereas that to the northeast (NE) is redshifted, consistent with gas orbiting in a disk inclined with respect to the plane of the sky. With a beam size of ~2″ (or 280 AU), the OVRO CO 2 → 1 image of the LkCa 15 disk is well resolved. A Gaussian fit to the velocity-integrated CO intensity map (Fig. 2) results in a FWHM of $(4\farcs4 \pm 0\farcs4) \times (3\farcs6 \pm 0\farcs3)$ at a position angle of 68°, which corresponds to a radius of $\gtrsim$300 AU.

At such moderately large inclinations, shear broadening exceeds thermal broadening in the spectrum, and the local emissivity of optically thin lines becomes anisotropic (Horne & Marsh 1986). In this case, the separation of the two peaks in the CO 2 → 1 spectrum (2.6 km s^{-1}; see Fig. 3) becomes $2v_{\rm Kep} \sin i$, where $v_{\rm Kep}$ is the Doppler shift due to the Keplerian orbital motion, or $(GM_*/R_d)^{1/2}$, indicating $R_d \gtrsim 313$ AU. In Figure 4, observed maps on velocity channels of width 0.65 km s^{-1} are compared with synthetic maps generated by a detailed model of a disk in Keplerian rotation. Following Koerner (1995; see also Mannings, Koerner, & Sargent 1997), the model used a two-component Gaussian emissivity distribution with half-maximum radii taken from the fit to the integrated intensity map in Figure 2. The inclination angle i, outer cutoff radius R_d, and relative amplitudes of the Gaussian components were varied to match the structure in Figure 4. Best fits were found for a central mass $0.9 \pm 0.2\ M_\odot$ and disk inclination of $i_{\rm disk} = 58° \pm 10°$. The outer Gaussian component has a HWHM of 425 AU and a cutoff radius of 750 AU. These values are in good agreement with optical and infrared photometry (Bouvier et al. 1995), Plateau de Bure Interferometer (PdBI) CO observations (Simon et al. 2001) and with our resolved 1.2 mm continuum observations. As can be seen in Figure 4, synthetic maps produced from this model agree very well with the CO $J = 2 \rightarrow 1$ spectral line maps of LkCa 15. The size of the gas disk is thus well determined from both the image and the spectral data cube and is much larger than the dust disk size as determined from continuum emission. In what follows, important disk physical properties are fixed at the values derived from the dust (disk mass) and CO (disk size and orientation) emission.

For robust measurements of the abundance and excitation of CO, it is necessary to derive observational estimates of line opacities. These can be obtained by examining a range of transitions and isotopologues. Visibilities from several configurations were therefore combined to examine the ^{13}CO, C^{18}O, HCO$^+$, and N_2H^+ $J = 1 \rightarrow 0$ transitions; results are presented in Figures 5 and 6. The velocity patterns observed in both ^{13}CO and HCO$^+$ are entirely consistent with those seen in CO, with redshifted emission to

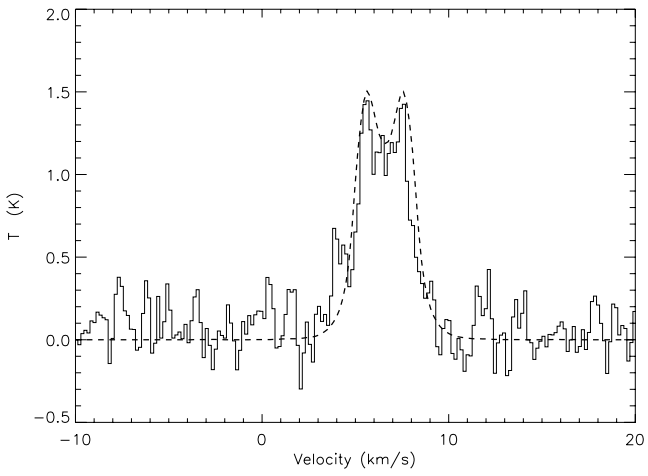

FIG. 3.—Disk-averaged spectrum of CO 2 → 1 (*solid histogram*), compared with the model CO emission for a 430 AU radius disk inclined at 58° (*dotted line*). Details of the calculation can be found in § 3.2.

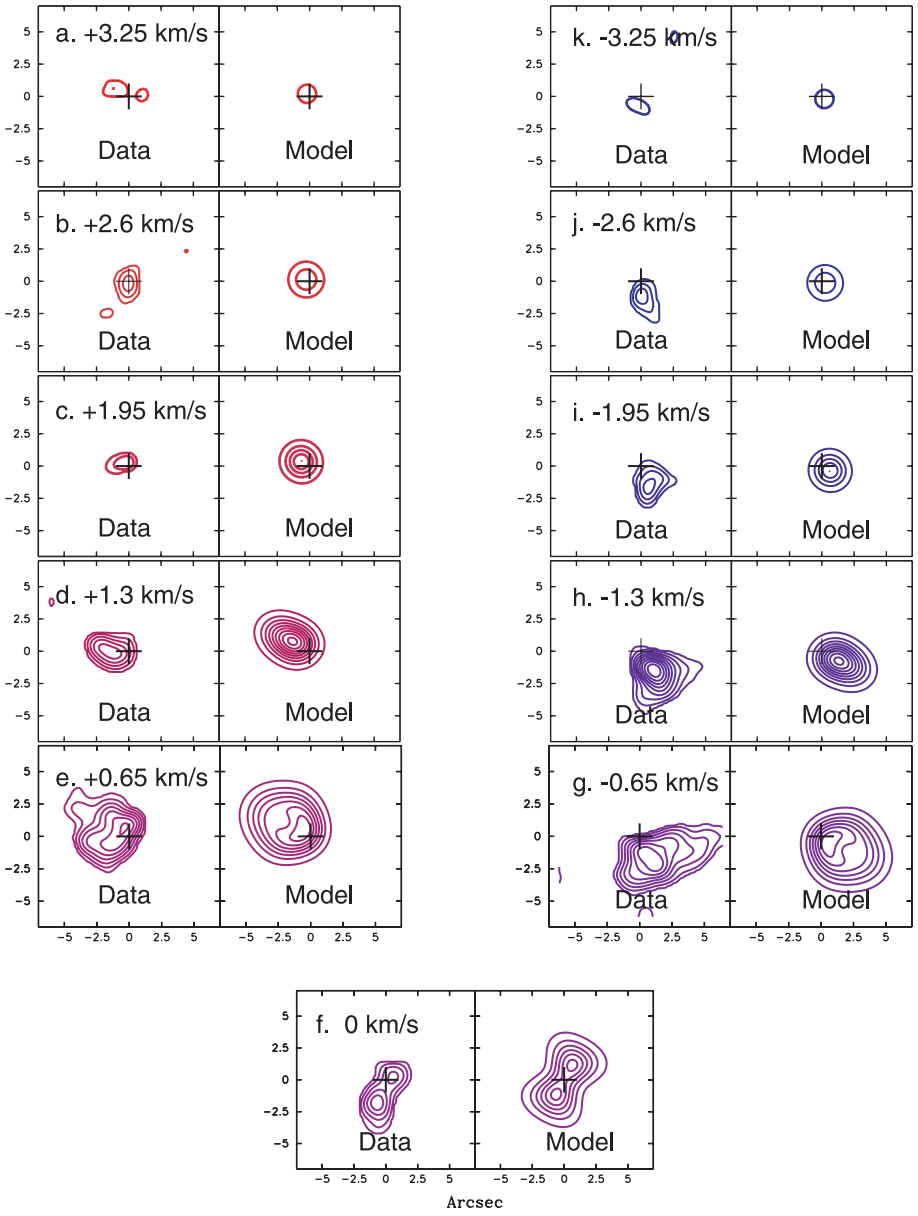

FIG. 4.—Spectral-line maps of the CO 2 → 1 emission toward LkCa 15, obtained with OVRO in steps of 0.65 km s^{-1}, shown adjacent to simulations of the emission predicted by a kinematic model of a disk in Keplerian rotation with parameters as described in the text. The velocities are referred to the stellar (systemic) velocity of $v_{\rm LSR} = 6.3$ km s^{-1}.

the NE and blueshifted emission to the SW. The $C^{18}O$ and N_2H^+ 1 → 0 data cubes have lower signal-to-noise values, and so no velocity analysis was carried out for these transitions. The integrated line intensities and the corresponding column densities for the above transitions were derived with the assumptions of local thermodynamic equilibrium (LTE) and optically thin emission at an excitation temperature of 30 K as presented in Table 1. Only upper limits have been obtained for $H^{13}CO^+$.

3. DISCUSSION

3.1. *Disk Structure and Grain Properties*

Two of the most important global properties of a disk are its mass and temperature distribution. At sufficiently short wavelengths, the entire disk is optically thick, and the density distribution does not affect the emission. At wavelengths longer than about 300 μm, however, the thermal emission from circumstellar disks becomes optically thin. Thus, continuum observations at millimeter wavelengths provide an excellent way to measure disk masses directly via the equation

$$F_\nu = \int I_\nu d\Omega = \int S_\upsilon \tau_\upsilon \, d\Omega \approx \int \frac{2kT}{\lambda^2}\kappa_\nu \, \Sigma \, d\frac{\sigma}{D^2} = \frac{2k\langle T\rangle}{\lambda^2 D^2}\kappa_\nu M \, , \quad (1)$$

where $M = \int \Sigma \, d\sigma$, F_ν is the flux density, κ_ν is the mass opacity, Σ is the surface density, and σ is the surface area of the disk (Beckwith et al. 1990). The dust temperatures T are almost always sufficiently high (typically 50 K) to make the Rayleigh-Jeans assumption valid, so the total emission is proportional to a product of the total mass and the average

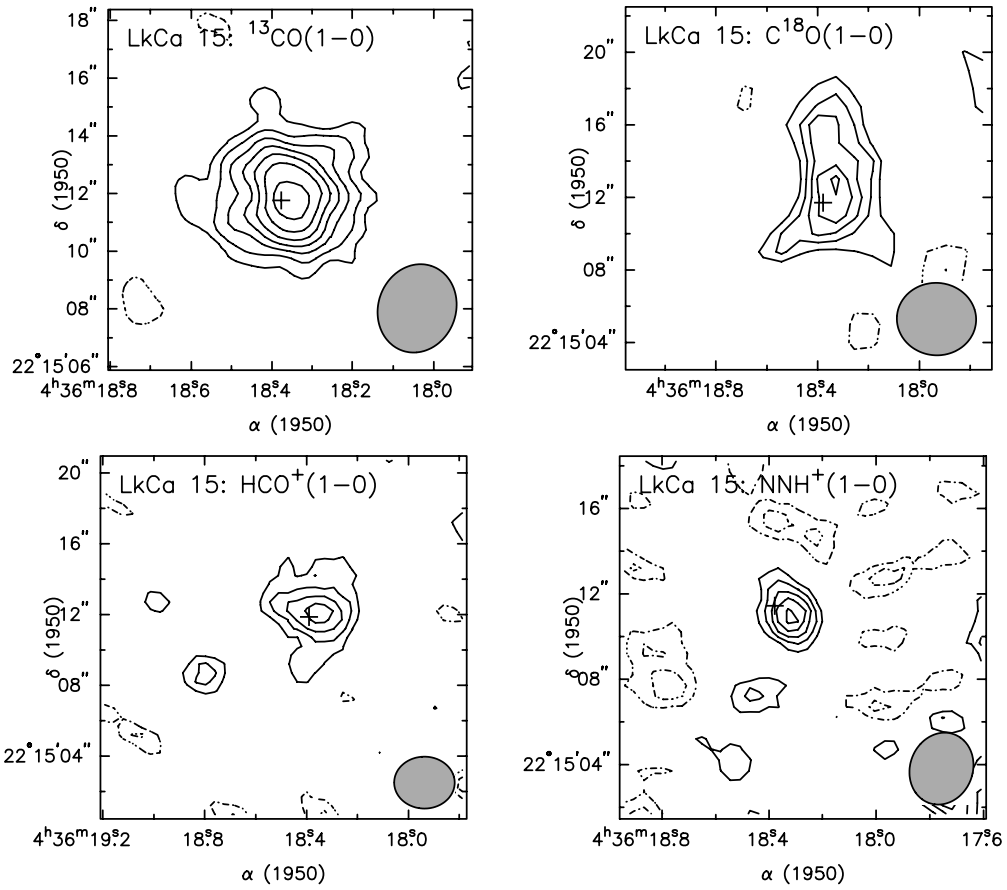

FIG. 5.—*Top*: Integrated intensity maps of ^{13}CO (*left*; contours start at 0.16 and are spaced by 0.08 Jy beam^{-1} km s^{-1}) and C^{18}O (*right*; contours start at 0.1 and are spaced by 0.05 Jy beam^{-1} km s^{-1}) $1 \rightarrow 0$ emission. *Bottom*: Integrated intensity maps of HCO$^+$ (*left*; contours start at 0.16 and are spaced by 0.08 Jy beam^{-1} km s^{-1}) and N$_2$H$^+$ (*right*; contours start at 0.1 and are spaced by 0.05 Jy beam^{-1} km s^{-1}) $1 \rightarrow 0$ emission. All steps correspond to the rms noise level in each map.

temperature $\langle T \rangle$, weighted appropriately by its radial distribution. The major uncertainty in mass estimates arises from κ_ν. Theoretically, κ_ν is expected to vary as a power of the frequency ν: $\kappa_\nu = \kappa_0(\nu/\nu_0)^\beta$. Following Beckwith et al. (1990), we adopt a fiducial value of $0.02(\nu/230\ \mathrm{GHz})\ \mathrm{cm}^2\ \mathrm{g}^{-1}$ and calculate the total gas mass assuming $M_{\mathrm{gas}}/M_{\mathrm{dust}} = 100$. The disk mass of LkCa 15 is calculated to be $\sim 0.01\ M_\odot$.

More detailed constraints for the density and temperature structure can be derived by fitting the spectral energy distributions (SED) of young star/disk systems. Figure 1 shows the flux density as a function of frequency of the millimeter wavelength emission from LkCa 15. Because the continuum and molecular lines were observed simultaneously, the frequencies of the continuum observations at 1.3 and 2.7 mm vary slightly, depending on the local oscillator frequency required for the molecular line observations. In Figure 1, the spectral index, α, as defined by $F_\nu \approx \nu^\alpha$, is 2.65, consistent with IRAM PdBI observations (Duvert et al. 2000). A separate analysis of the data in each atmospheric window, however, suggests that the slope of the 3 mm points alone ($\alpha = 3.51$) is considerably steeper than that for the 1.3 mm fluxes ($\alpha = 2.34$), although the error bars are large.

In order to examine this issue further, we compare our OVRO 3.4–1.2 mm continuum fluxes with those obtained at 870 μm and 7 mm by the James Clerk Maxwell Telescope (JCMT) and the Very Large Array (VLA), respectively. The JCMT SCUBA flux lies along a spectral index α of 2.65 with

TABLE 1
OBSERVED MOLECULAR INTENSITIES AND COLUMN DENSITIES TOWARD LkCa 15

Transition	Beam (arcsec)	$\int Tdv$ (K km s^{-1})	N(30 K, LTE) (cm^{-2})	N(model) (cm^{-2})	Model Ratios N(model)/N(30 K, LTE)
CO $2 \rightarrow 1$	1.81×1.49	12.5	7.28(15)	1.68(18)	230
^{13}CO $1 \rightarrow 0$	2.74×2.41	6.39	1.11(16)	3.04(16)	2.74
C^{18}O $1 \rightarrow 0$	5.05×3.59	1.90	3.31(15)	1.40(15)	0.42
HCO$^+$ $1 \rightarrow 0$	7.74×5.64	3.30	9.25(12)	2.31(13)	1.79
H^{13}CO$^+$ $1 \rightarrow 0$	6.30×4.41	<0.88	$<2.60(12)$	$<1.12(12)$	0.43
N$_2$H$^+$ $1 \rightarrow 0$	3.51×3.17	3.83	1.71(13)	3.07(13)	1.80

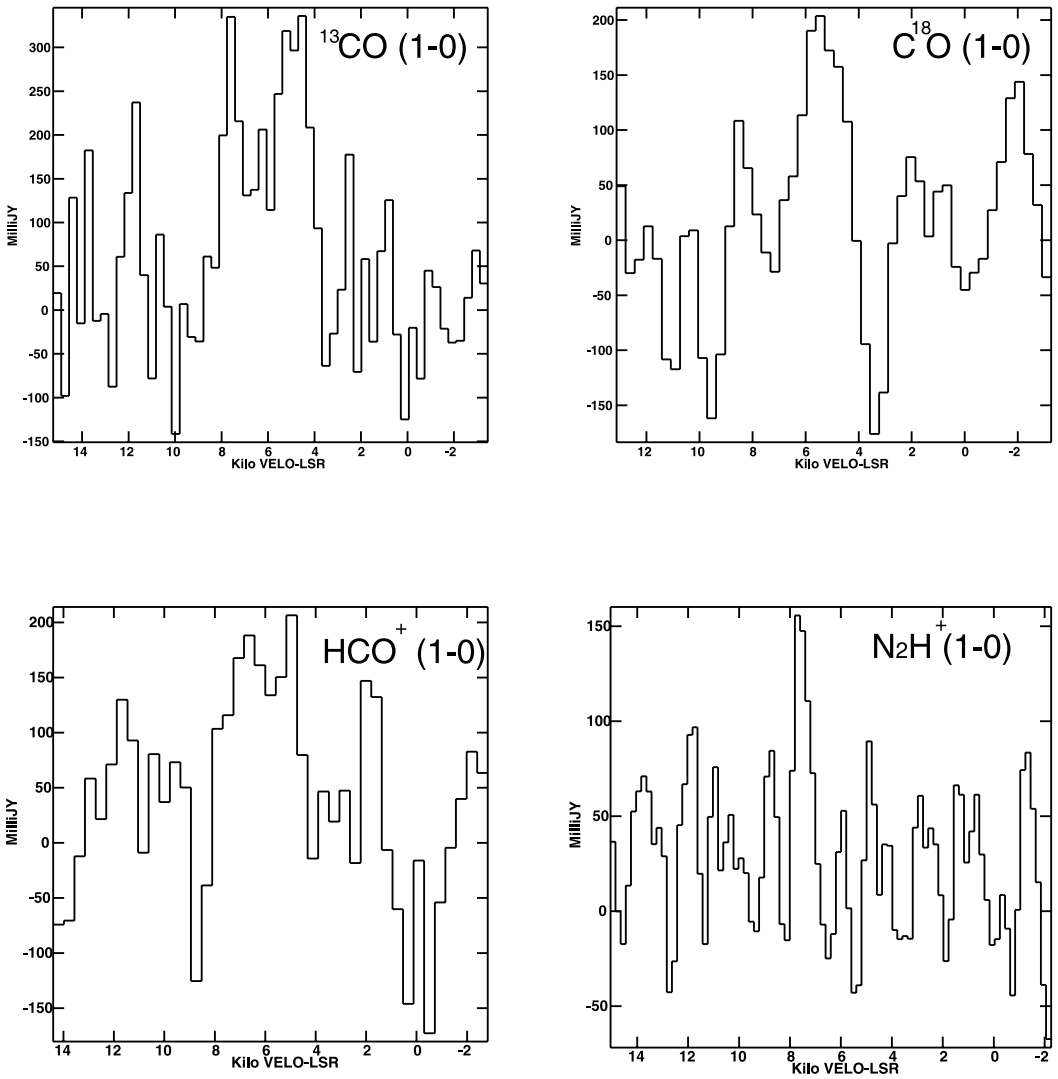

FIG. 6.—Disk-averaged spectra of the molecules in Fig. 5, obtained over boxes of $6'' \times 7''$ for ^{13}CO, $8'' \times 5''$ for $C^{18}O$, $6'' \times 7''$ for HCO^+, and $6'' \times 6''$ for N_2H^+.

respect to the OVRO data and so is consistent with the local slope derived from the OVRO 1.3 mm continuum emission measurements. No simple extrapolation of the submillimeter data can explain the VLA nondetection at 7 mm (D. Wilner 2003, private communication), which requires α values similar to or even larger than those measured at 3 mm. The coincidence of the 1.3 and 3 mm data observed by Duvert et al. (2000) with the fits to our OVRO data indicate that the observed change in the spectral index at millimeter wavelengths is not likely to be due to errors in flux calibration.

Several physical mechanisms, notably optical depth effects and grain growth, can contribute to the observed behavior. As mentioned above, κ_ν is expected to vary as ν^β, where β is the opacity index. Assuming optically thin emission in the Rayleigh-Jeans limit, the opacity index β $(=\alpha - 2)$ varies from 1.51 to 0.34 for the LkCa 15 disk, while β is approximately 2 for dust in the diffuse interstellar medium.

How reasonable is this assumption of optically thin continuum emission? Following Beckwith et al. (1990),

$$\alpha - 2 = \beta/1 + \{p/[2 - q]\ln[2/(2 - p)\tau]\}\ , \qquad (2)$$

where $\{p/[2 - q]\ln[2/(2 - p)\tau]\}$ is the ratio of optically thick to optically thin emission and depends on the disk structure, $\tau_\nu = (\kappa_\nu M_D)/\left(\cos\theta\pi R_D^2\right)$ is the average optical depth at frequency ν, and M_D is the mass of the disk. Given the dust disk radius of 190 AU and an M_D of 0.01 $M_\odot$ (derived above from F_ν), the average optical depth at 230 GHz is $\lesssim 0.03$. Thus, for any reasonable disk density and temperature distribution, the optical depth correction does not appear to be sufficient to explain the observed change in the LkCa 15 spectral index with a single β.

One means to solve this dilemma is for the mass opacity coefficient κ_ν to decrease by nearly an order of magnitude between 1.2 and 3.4 mm. Recent detailed models of irradiated T Tauri disks, including dust grain growth (D'Alessio, Calvet, & Hartmann 2001), conclude that when grains grow from μm to mm sizes, the mass opacity coefficient κ_ν changes significantly between 1.3 and 3 mm. Indeed, observations of circumstellar disks (Beckwith et al. 1990; Mannings & Emerson 1994; Wilner, Ho, & Rodriquez 1996) indicate typical values of β around 0.3, similar to that expected from mm-sized pebbles $(0 < \beta < 2)$, as opposed to the steeper frequency

dependence of κ_ν ($\beta = 2$) found in the general interstellar medium (Hildebrand 1983).

As indicated by Chiang et al. (2001), the disk mass and grain size distribution cannot be uniquely constrained by the continuum SED alone when only unresolved fluxes are available. Additionally, D'Alessio et al. (2001) find that for a given total dust mass, grain growth is accompanied by a decrease in the vertical height of the disk surface. Fits of the SED for LkCa 15 (Chiang et al. 2001) indicate that the ratio of the height of the disk photosphere (H) to the vertical gas scale height (h) is small (1.0), which can be interpreted as evidence that the dust has begun to settle vertically toward the midplane. The H/h parameter is a rather robust one within the confines of the model, for as H/h decreases from 4 to 1, there is a corresponding decrease in the overall level of infrared excess at $\lambda \leq 100$ μm, since the disk intercepts less stellar radiation. Dust settling can help explain the relative paucity of large disks to which the powerful technique of scattered light coronography can be applied and, specifically, the lack of any detectable reflection nebulosity in *HST* WFPC2 GTO observations of LkCa 15 (Krist et al. 1997). Thus, the most likely explanation for the observed change in the spectral index from 1 to 3 mm is a combination of grain growth and dust settling.

3.2. *Radiative Transfer and Molecular Line Emission*

The observed line intensities in circumstellar disks are a complex function of the physical structure of the disk and of the line/continuum optical depth. If we assume that circumstellar disk abundances are similar to those found in dark clouds, the emission lines from parent isotopologues of common species such as CO, HCO^+, HCN, etc., should be highly optically thick. Our observed ratios of $^{12}CO/^{13}CO$ emission reveal that ^{12}CO is indeed optically thick but say little about ^{13}CO. Several LkCa 15 transits were therefore devoted to a local oscillator setting containing the $C^{18}O$ $J = 1 \rightarrow 0$ transition, the results of which are presented in Figure 5. The observed beam-matched flux density ratio is 5, only somewhat lower than the isotope ratio $[^{13}C]/[^{18}O]$ of 8.3. The ^{13}CO $J = 1 \rightarrow 0$ transition is therefore only somewhat optically thick, and that of $C^{18}O$ is optically thin and should provide a more reliable estimate of the disk mass, *provided* it remains in the gas phase. Van Zadelhoff et al. (2001) indicate that for standard HCO^+ abundances, the $1 \rightarrow 0$ line is again optically thick in the outer layers, whereas that of $H^{13}CO^+$ is close to being optically thin throughout the disk. Further, the low-J HCO^+ lines are predicted to probe densities of the order of 10^5–10^6 cm^{-3}, below the critical density of the $4 \rightarrow 3$ transition (so that LTE cannot be safely assumed). For $H^{13}CO^+$, the populations will be closer to thermal equilibrium because its emission arises primarily from regions with densities of 10^7–10^8 cm^{-3} (van Zadelhoff et al. 2001). Parent isotopologue lines are therefore likely to be optically thick for many species in disks, and so whenever possible, the emission from isotopically substituted species should be utilized in deriving relative molecular abundances.

The observations described above indicate the need for detailed calculation of disk radiative transfer. Furthermore, the complex geometry within the disk demands that flexible and efficient radiative transfer techniques be utilized, and of the many techniques available, the Monte Carlo approach has shown great promise (Choi et al. 1995). Since Monte Carlo techniques utilize integration paths chosen at random, any number of coordinate systems can be used. The high optical depth of many transitions in circumstellar disks generates very short photon mean free paths, however, and so unless aggressive acceleration schemes are employed, the Monte Carlo approach can be very slow. Computational instabilities and poor convergence can result, but efficient one-dimensional and two-dimensional Monte Carlo treatments of the line radiative transfer based on the two-layer passive disk models outlined above have now begun to appear (Hogerheijde & van der Tak 2000; van Zadelhoff et al. 2001). In all such approaches, the intensity of each line is calculated by solving the radiative transfer equation.

Two-dimensional implementations are necessary to quantitatively treat inclined disks. For this reason, we have used an accelerated two-dimensional Monte Carlo model (Hogerheijde & van der Tak 2000) to examine the radiative transfer and molecular excitation in the LkCa 15 disk, taking both collisional and radiative processes into account. This model produces a simulated observation of each transition as imaged by a telescope with infinite resolution for a disk of a given size, inclination, and temperature distribution. The MIRIAD function UVMODEL and the observed visibility data set were then used to sample this model at the observed (u, v) spacings, and the model data set was processed in a manner identical to that of the OVRO data, thus allowing a direct comparison of the two. For these model calculations, the temperature and hydrogen density as a function of radius and height were acquired from a model similar to those presented in D'Alessio et al. (2001) but calculated specifically for the stellar parameters of LkCa 15 such that the overall SED of the star+disk is reproduced. In this model, we assume spherical, compact dust grains with a power-law size distribution with exponent 3.5, a maximum grain size of 1 mm, and grain abundances from Pollack et al. (1994). The accretion rate is assumed to be 1.0×10^{-8} $M_\odot$ yr^{-1}, with the inner radius of the disk set at 5 AU and the outer radius at 425 AU, which is consistent with that derived above for LkCa 15. The inclination (58°) and turbulent velocity width (0.1 km s^{-1}) are found by fitting the observed CO $2 \rightarrow 1$ line profile with the model spectrum, using $N_{CO} = 10^{-4} N_H$,[6] as shown in Figure 3. For each transition observed, a suite of models with the parameters described above was created, but with the molecular abundances relative to hydrogen varied until a match with the observed integrated line intensity was obtained. Integrated intensity is a useful quantity for comparison because the column density is approximately constant as a function of radius (Willacy & Langer 2000; Aikawa & Herbst 1999) at the large radii (>50 AU) to which we are sensitive with the OVRO Millimeter Array.

The resulting column densities are shown in Table 1. The column densities calculated using this non-LTE radiative transfer model are 1–2 orders of magnitude larger than those calculated in the Willacy & Langer (2000) models of disk chemistry but consistent with those calculated by Aikawa et al. (2002), except that N_2H^+ is an order of magnitude larger than the model prediction. As indicated in the

[6] This model assumes that CO and H_2 have similar radial and vertical distributions. Chemical models (e.g., Aikawa et al. 2002) indicate that this is not strictly the case, and variations in the vertical distribution of CO will be explored in future work.

last column of Table 1, for CO $2 \rightarrow 1$, ^{13}CO $1 \rightarrow 0$, HCO^+ $1 \rightarrow 0$, and N_2H^+ $1 \rightarrow 0$ emission, the column densities are smaller when calculated using the LTE assumption. This is due to the fact that the emission from these transitions is optically thick (see discussion above). The LTE calculations assume that the gas is optically thin and that the entire disk is being probed by observation of this line emission, and thus result in an underestimation of the total amount of CO, HCO^+ and N_2H^+ present. In the case of the $C^{18}O$ $1 \rightarrow 0$ and $H^{13}CO^+$ $1 \rightarrow 0$ emission, which are believed to be optically thin, and for the conditions in the near-surface regions of disks beyond 50 AU, the column densities are overestimated when thermal equilibrium is assumed. This supports the conclusion that conditions in the emitting region are not at LTE and that both radiative and collisional processes play a part in the excitation. The population of higher energy rotational states is thus much lower than would be the case if collisions were dominant, and the assumption of thermal equilibrium therefore results in an overestimation of the population of the upper states and, thus, in the total column density, which at LTE is directly proportional to the density of the upper state.

Both the results presented above and observations of high-J transitions of CO, HCO^+, and HCN toward LkCa 15 by van Zadelhoff el al. (2001) suggest that the molecular emission from the major isotopologues is optically thick and that the inferred densities in the region are not sufficient to thermalize all transitions. The line ratios presented in van Zadelhoff el al. (2001) further indicate temperatures and densities typically associated with warm layers lying above the disk midplane. Additionally, if we ignore depletion of gas-phase species onto grains and assume cosmic fractional abundances for CO (10^{-5}–10^{-4} N_H) and hydrogen column densities of 10^{23} cm^{-2}, the resulting CO column density is an order of magnitude greater than that observed here (10^{18} cm^{-2}). Thus, for any disk in which the gas and dust are well mixed and there is no depletion, even species such as $C^{18}O$ are predicted to be optically thick at molecular cloud abundances. The low column densities derived here and the high-J/low-J line ratios therefore indicate that the disk midplane (heights below several tens AU) is not being probed by the observed emission and that the column densities presented in Table 1 are only applicable to the warm layers of the disk.

3.3. *Ionization Balance*

The theory of the ionization balance in molecular clouds and the relevant ion-molecule chemistry has been widely used for determinations of the electron abundances in dense clouds (Langer 1985). Theoretical chemical models indicate that ion-molecule reactions are also efficient in the outer regions of protoplanetary disks (Aikawa et al. 1998). Photoionization, cosmic ray ionization and, possibly, X-ray ionization of H_2 rapidly lead to the formation of H_3^+, the pivotal species in ion-molecule models of molecular cloud chemistry. The low proton affinity of H_2 ensures that H_3^+, which has no rotational spectrum, will undergo proton transfer reactions with abundant neutral species such as CO and N_2. In disks, gaseous CO and N_2 exist in regions well removed from the midplane, where the temperature warms enough for sublimation of these molecules ($T \approx 20$–30 K). The isoelectronic ions HCO^+ and N_2H^+ were observed here and can therefore be used to estimate the fractional ionization in the warm layer of the LkCa 15 disk.

The volume density in the emitting region can be constrained from line ratios obtained from the results presented here and previous single-dish observations of molecules with high dipole moments (e.g., HCO^+, HCN). An LVG analysis for LkCa 15, performed by van Zadelhoff et al. (2001), indicates that the lines arise from regions with $n_{H_2} \sim 10^5$–10^7 cm^{-3}. We use 10^6 cm^{-3} as the number density of H_2 in the calculations below, which is also the number density at a height of $\sim$150 AU and a radius of 350 AU in the D'Alessio disk model. The mean kinetic temperatures are less well constrained, but the analysis of multiple transitions of CO (van Zadelhoff et al. 2001) suggests that $T_{kin} \sim 20$–40 K for LkCa 15. We therefore adopt a single kinetic temperature of 30 K. Also, for the reasons discussed in § 3.2, we use the column densities resulting from the non-LTE radiative transfer model summarized in Table 1 for all observed species. Because H_2 cannot be observed directly at millimeter wavelengths, the column density is highly model-dependent. Typical values vary from 10^{23} to 10^{24} cm^{-2} for $R \sim 300$ AU, the distance corresponding to the typical beam size of our observations. Van Zadelhoff et al. (2001) investigate the level of molecular depletion by statistical equilibrium calculations as compared to the gas column densities predicted by dust continuum observations and find depletion by a factor of 3–40 for CO in the disk of LkCa 15. We therefore adopt 10^{-5} as the fractional abundance of CO by assuming depletion by a factor of 10 from the nominal value of f(CO) in molecular clouds. In our calculations, we also assume that the warm layers in the disk are in local (chemical) equilibrium and that the abundances of CO, HCO^+, and N_2H^+ peak within these layers (Aikawa et al. 2002), although the vertical distributions of these species are not identical (cf. Fig. 4 of van Zadelhoff et al. 2003 and Figs. 4 and 5 of Willacy & Langer 2000).

To simplify the calculations presented here, we first consider only the ionization balance determined by HCO^+, H_3^+, N_2H^+, and electrons in steady state, for which

$$k_1[H_3^+][CO] = k_e(HCO^+)[HCO^+][e] - k_2[N_2H^+][CO] , \quad (3)$$

$$k_e(H_3^+)[H_3^+][e] + k_3[N_2][H_3^+] + k_1[H_3^+][CO] = \frac{\zeta}{n(H_2)} , \quad (4)$$

$$k_3[N_2][H_3^+] = k_2[N_2H^+][CO] + k_e(N_2H^+)[N_2H^+][e] , \quad (5)$$

where

$$k_e(H_3^+) = 1.15 \times 10^{-7}(T/300)^{-0.65} \text{ cm}^3\text{s}^{-1} ,$$
$$k_e(HCO^+) = 2.0 \times 10^{-7}(T/300)^{-0.75} \text{ cm}^3\text{s}^{-1} , \quad \text{and}$$
$$k_e(N_2H^+) = 1.7 \times 10^{-7}(T/300)^{-0.9} \text{ cm}^3\text{s}^{-1}$$

are the dissociative recombination rate coefficients of H_3^+, HCO^+, and N_2H^+, $k_1 = 6.56 \times 10^{-10}(T/300)^{-0.5}$ cm^3 s^{-1} and $k_2 = 8.8 \times 10^{-10}$ cm^3 s^{-1} are the reaction rate coefficients of CO with H_3^+ and N_2H^+, respectively, $k_3 = 1.8 \times 10^{-9}$ is the rate coefficient for the reaction $N_2 + H_3^+ \rightarrow N_2H^+ + H_2$ (all rate coefficients have been adopted from the UMIST database for astrochemistry; Millar, Farquhar, & Willacy 1997), and the bracket [ ] represents the fractional abundance of the species and ζ the ionization rate due to cosmic rays, X-rays, and UV radiation.

A lower limit to the electron fraction follows directly from the observed HCO^+ and N_2H^+ column densities but can also be obtained more locally by noting that the right

side of equation (3) must be larger than 0, or

$$\frac{[e]}{[\mathrm{CO}]} \geq \frac{k_2[\mathrm{N_2H^+}]}{k_e(\mathrm{HCO^+})[\mathrm{HCO^+}]} \sim 1 \times 10^{-3} . \quad (6)$$

The lower limit of the fractional ionization $[e]$ is therefore $\gtrsim 10^{-8}$, given $[\mathrm{CO}] \sim 10^{-5}$ in the near-surface region of the disk. This value is fairly high compared to that of cold, dark clouds at $n_{\mathrm{H_2}} \sim 10^6$ cm^{-3}, where, for example, Caselli et al. (2002) obtained fractional ionization of 10^{-9} in the center of L1544, and we note that the ionization fraction in LkCa 15 may be enhanced relative to other T Tauri stars. The *ROSAT* All-Sky Survey of young stars in Taurus (Neuhaeuser et al. 1995) shows that the probability of the existence of an X-ray source for LkCa 15 is 98% and the upper limit for its X-ray luminosity is 4.1×10^{29} ergs^{-1}. Ionization from the resulting high-energy radiation may have important effects on the disk (Feigelson & Montmerle 1999). The high $\mathrm{HCO^+}$ abundance and CN/HCN ratio observed (Qi, Kessler, & Blake 2003, in preparation) indicate that LkCa 15 could possess similar chemistry to the intense X-ray source TW Hya, another Sun-like star with strong molecular emission from its attendant disk (Kastner et al. 1997).

Understanding the ionization rate near the disk surface is important because the electron fraction scales linearly with the ionization rate. A full three-dimensional calculation of X-ray transport and ionization in axially asymmetric disks has been developed by Igea & Glassgold (1999) using a Monte Carlo approach. They calculate the ionization rate at $R = 1$ AU in a minimum mass solar nebula disk model with $L_{\mathrm{X}} = 10^{29}$ ergs s^{-1}, which can be scaled to other X-ray luminosities and disk radii and is found to be relatively insensitive to changes in disk parameters. Scaling their values at $R = 300$ AU with $N(\mathrm{H_2}) \sim 10^{23}$ cm^{-2}, we calculate an X-ray ionization rate of $\sim 10^{-16}$ s^{-1} near the surface of the LkCa 15 disk. This is nearly a factor of 10 larger than the galactic cosmic ray ionization rate and shows that X-rays can play an important role in the disk ionization balance. The enhanced ionization can drive additional chemical activity, and the inclusion of X-rays within the context of dust settling models developed for LkCa 15 may well account for much higher abundances of molecules observed toward this source as compared with the DM Tau disk, for which standard disk chemistry models produce good agreement with observations (Aikawa et al. 2002).

By considering the balance of all the molecular ions present in the disk, even tighter constraints can be placed on the electron fraction. We consider two conditions with differing abundances of metal ions, as discussed in Langer (1985). When the abundances of metal ions are low, $\mathrm{H_3^+}$, $\mathrm{HCO^+}$, and $\mathrm{N_2H^+}$ become the major cations within the disk. Because $\mathrm{HCO^+}$ and $\mathrm{N_2H^+}$ have fractional abundances that are only $\gtrsim 10^{-10}$ while the lower limit to the electron fraction is closer to 10^{-8}, $\mathrm{H_3^+}$ dominates. In this case, the electron abundance can be calculated simply from $[e] \simeq \{\zeta/[k_e n(\mathrm{H_2})]\}^{1/2} \sim 1.4 \times 10^{-8}$ (Langer 1985), which yields values similar to those derived above. However, the high resulting abundance of $\mathrm{H_3^+}$ drives rapid protonation of CO, i.e., $k_1[\mathrm{H_3^+}][\mathrm{CO}] \gg k_e(\mathrm{HCO^+})[\mathrm{HCO^+}][e]$, and makes $\mathrm{HCO^+}$ balance (eq. [3]) impossible within the confines of the simple model.

It is therefore reasonable to examine the contribution of metal ions to the fractional ionization because they are destroyed very slowly and can comprise a significant fraction of the ion abundance, even though their elemental abundances are small. Fromang, Terquem, & Balbus (2002) calculate the ionization fraction of protostellar disks, taking into account vertical temperature structure and the possible presence of trace metal atoms, and find that a tiny fraction of the cosmically available metals can dramatically affect the ionization balance. Considering the model above, but now with $[\mathrm{H_3^+}] + [\mathrm{HCO^+}] + [\mathrm{N_2H^+}] \ll [e]$, we can solve for the three unknown variables $[\mathrm{N_2}]$, $[\mathrm{H_3^+}]$, and $[e]$ in order to balance equations (3), (4), and (5). Using equations (4) and (5), removing the term $k_3[\mathrm{N_2}][\mathrm{H_3^+}]$ and inserting the value of $\mathrm{H_3^+}$ derived from equation (3), the equation for $[e]$ becomes

$$k_e(\mathrm{HCO^+})k_e(\mathrm{H_3^+})[\mathrm{HCO^+}][e]^2 + B[e] - \frac{\zeta}{n(\mathrm{H_2})}k_1[\mathrm{CO}] = 0 , \quad (7)$$

where

$$B = -k_2k_e(\mathrm{H_3^+})[\mathrm{CO}][\mathrm{N_2H^+}] + k_1k_e(\mathrm{HCO^+})[\mathrm{CO}][\mathrm{HCO^+}] + k_1k_e(\mathrm{N_2H^+})[\mathrm{CO}][\mathrm{N_2H^+}] .$$

This equation can be solved using the observed column densities of CO, $\mathrm{HCO^+}$, and $\mathrm{N_2H^+}$ and an assumed density of $\mathrm{H_2}$. The $\mathrm{N_2}$/CO ratio can also be derived from equations (5) and (7) under such conditions, and Figure 7 presents the solutions for a range of $\mathrm{H_2}$ column densities. Not surprisingly, the electron fraction is calculated to be larger than the metal-free case ($\sim 10^{-8}$), which, as we stress above, can only be applied for the physical conditions prevailing near the warm surface layer(s) of the disk.

Transport processes in the outer disk likely depend critically on the degree of ionization. Efficient coupling between the neutral material and magnetic fields is thought to be provided by fractional ionizations of $\gtrsim 10^{-8}$ (Feigelson & Montmerle 1999). As we have outlined above, photons, X-rays, and cosmic rays can be important sources of ionization near the disk surface. The photon penetration depth is very short compared to the disk thickness, however, and even cosmic rays are exponentially attenuated for columns greater than 100 g cm^{-2}. The electron fraction can therefore

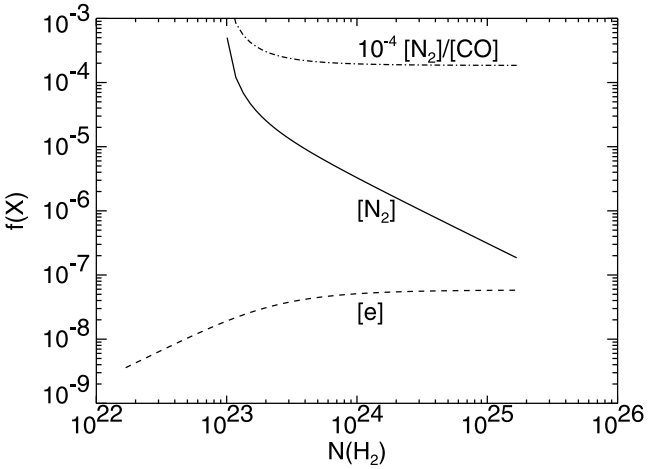

FIG. 7.—Fractional abundances $[f(\mathrm{X}) = N(\mathrm{X})/N(\mathrm{H_2})]$ of $\mathrm{N_2}$ and electrons vs. the $\mathrm{H_2}$ column density for the simple fractional ionization model discussed in § 3.3.

be expected to drop toward the midplane due to the increasing density, suggesting the possibility of layered accretion (Gammie 1996) with a turbulent surface layer. However, due to the depletion of volatiles such as CO, the disk midplane fractional ionization may be larger than expected from a direct extrapolation of the electron abundance inferred for the surface layer. For very high depletions, electron recombination begins to control the fractional abundance of H_3^+, resulting in a higher than expected electron (and H_3^+) abundance. The details of the vertical and radial ionization fraction are pivotal to magnetohydrodynamic (MHD) models of young stellar object accretion disk viscous transport mechanisms (Glassgold, Feigelson, & Montmerle 2000). Balbus & Hawley (1991), for example, propose that differential rotation drives instabilities in the perpendicular magnetic field of accretion disks. Such magnetorotational instabilities then create a turbulent disk if they are well coupled to the neutral disk material. As shown above, observations suggest that the combination of photons, X-rays, and cosmic rays can produce the ionization needed to couple the magnetic field to the neutral disk material near the disk surface. Chemically, transport or mixing processes between the surface layer and the disk interior would be necessary to bring freshly made molecules such as CN, HCN, or even deuterated species back to the interior of the disk. In this scenario, the extent of such processes, which are dependent on the ionization fraction, would greatly affect the composition of early solar system objects such as comets.

3.4. CO *Depletion and the* N_2/CO *Ratio*

If CO remains primarily in the gas phase, it is sufficiently chemically stable that its abundance will be little altered from dark cloud values. CO would therefore be a good tracer of the disk gas mass, but depletion onto grain mantles in the cold disk is likely to substantially reduce the *gas phase* column density of CO and many other species. Thus, estimates of the degree of depletion of volatile molecules such as CO and N_2 onto grains will greatly improve our understanding of disk chemistry. For CO, depletion factors can be measured directly from infrared spectroscopy of edge-on disks (Boogert, Hogerheijde, & Blake 2002), or more generally, by using observations of the dust continuum along with several isotopically substituted molecules (e.g., ^{12}CO, ^{13}CO, C^{18}O) to distinguish depletion from optical depth effects. From the column density of CO (1.7×10^{18} cm^{-2}) obtained with the detailed two-dimensional Monte Carlo radiative transfer model (Table 1), a disk gas mass of only $\sim 10^{-4}\ M_\odot$ is derived, a value in agreement with that derived from single-dish observations of ^{13}CO higher J transitions (Thi et al. 2001) using the JCMT and CSO, but nearly 2 orders of magnitude less than the mass derived from dust emission—far more than can be accounted for by errors either in the dust mass opacity coefficient or in the spectral line radiative transfer. Depletion thus appears to be a dominant effect, and while CO and its isotopomers are therefore excellent tracers of the disk velocity field, it is clear that they are not reliable tracers of the disk mass. In the models of Aikawa et al. (1996, 1999), CO depletes onto grains at radii greater than 200–300 AU. Inside this radius, the temperature warms to the sublimation temperature of CO ($T \sim 20$ K), and the gas phase column density rises substantially. If thermal sublimation is the main desorption mechanism, the depletion patterns in disks should be strongly correlated with volatility. We have observed strong emission from nonvolatile species such as HCN and CN toward LkCa 15 with spatial distributions that are not well correlated with CO (Qi, Kessler, & Blake 2003, in preparation). Additional mechanisms are therefore likely to be important in maintaining the observed gas-phase abundances.

As a closed shell homonuclear diatomic molecule, N_2 has no electric dipole allowed rotational transitions and so cannot be observed directly at millimeter wavelengths. However, from our N_2H^+ observations and the model presented above, we can estimate the N_2/CO ratio, and find it to be $\sim$2 (Fig. 7). This is much higher than the ratios inferred for typical dark clouds at moderate densities, which are $\sim$0.01–0.1 (Womack, Ziurys, & Wyckoff 1992; Bergin et al. 2001). In the dark cloud IC 5136, Bergin et al. (2001) do find evidence for the presence of differential gas-phase depletion and altered CO/N_2 ratios in the densest portions, where CO exhibits a significant abundance reduction and N_2H^+ is relatively undepleted, although in their models, the abundance of N_2 is still less than that of CO.

Within disks, Aikawa & Herbst (1999) investigated the two-dimensional chemical structure within the so-called Kyoto minimum mass solar nebula model (Hayashi 1981) and predicted much lower abundances of N_2 than CO at all vertical scales. Because they adopted an artificially low sticking probability to reproduce the spectra of CO available at that time, without specifying any nonthermal desorption processes or modifying the temperature distribution in the Kyoto model, such an approach might not account for the known differential desorption of CO and N_2. Further, the vertical temperature gradients of actual protoplanetary disks should be more complex than those in the Koyoto model (Chiang & Goldreich 1997; D'Alessio et al. 1997). Willacy & Langer (2000) investigated the molecules in the superheated layer of the Chiang & Goldreich (1997) disk models and found that molecules in this layer are destroyed by the harsh ultraviolet radiation from the star, although in the warm upper layers of the D'Alessio et al. models, UV shielding is sufficient to prevent destruction of most molecules (Aikawa et al. 2002). We therefore believe that N_2 and its chemical product N_2H^+ trace dense gas in the disk where CO is largely depleted but N_2 is not, and that this region is protected by an overlying warm layer that protects N_2 from ultraviolet radiation in order to produce the high N_2/CO ratio observed.

Deriving absolute fractional abundances is more difficult, but from the N_2/CO ratio and our Monte Carlo radiative transfer calculations, we estimate a fractional abundance for N_2 of $\sim 2 \times 10^{-5}$. N_2 would therefore represent a substantial fraction of the cosmically available nitrogen: this plus the gas phase N_2/CO ratio inferred for LkCa 15 provides a direct observational connection to comets. The abundance of N_2 in comets is an important guide to their volatile content because it is trapped and released by amorphous ice in a manner similar to that of Ar (Bar-Nun, Kleinfeld, & Kochavi 1988). This process has implications for understanding the role of comets for delivery of volatiles and noble gases to the terrestrial planets. Wyckoff, Tegler, & Engel (1991) have reviewed the total nitrogen abundance in comet Halley and argued that it is depleted by two- to sixfold relative to that of the Sun. The laboratory experiments performed by Bar-Nun et al. (1988) showed that CO is trapped 20 times more efficiently than N_2 in amorphous ice

formed at 50 K, and Owen & Bar-Nun (1995) predicted that in icy planetesimals forming in the solar nebula at about 50 K, $N_2/CO \approx 0.06$ in the gases trapped in the ice provided $N_2/CO \approx 1$ in the nebula itself, a value quite consistent with our data. Wyckoff & Theobald (1989) reported $N_2/CO \sim 2 \times 10^{-3}$ in Halley's comet, whereas Lutz, Womack, & Wagner (1993) found $N_2/CO \sim 2 \times 10^{-2}$ in comet Bradfield, and $N_2/CO \sim 3 \times 10^{-2}$ in comet Kohoutek. The observations are actually of the two molecular ions (CO^+ and N_2^+), and the conversion from the ion abundances to those of the neutrals is dependent on poorly constrained photodestruction branching ratios. Wyckoff & Theobald (1989) argued that the ion ratio must be multiplied by a factor of 2, while Lutz et al. (1993) find no factor necessary. Large amounts of gaseous N_2 may thus be required in the outer solar nebula, as we find in the disk of LkCa 15, in order to explain the N_2/CO ratios found in comets. This can be confirmed by measurements of the N_2/CO ratio in dynamically new comets, which should have higher values than those in short-period comets (Owen & Bar-Nun 1995).

4. SUMMARY

We have detected molecular gas and continuum emission from the disk encircling the T Tauri star LkCa 15 at frequencies between 85 and 260 GHz. The 1.2 mm dust continuum emission is resolved in our $1\farcs35 \times 0\farcs74$ beam with a minimum diameter of 190 AU and an inclination angle of $\sim 57°$. A noticeable decrease in the continuum spectral slope with frequency may result from the combination of grain growth and dust settling. Sensitive observations at longer wavelengths and submillimeter continuum images are needed to confirm the trend. On the basis of Keplerian rotation model fits to the CO velocity field, the gas emission extends to $\sim$750 AU, while the characteristic radius of the disk is determined to be closer to 425 AU from Gaussian fits to the CO $2 \rightarrow 1$ spectral data cube.

We have also presented molecular images of various isotopologs of CO and the HCO^+ and N_2H^+ ions in the disk. Our observations show that most of the molecular emission from the dominant species of common molecules is optically thick. Different molecules and even different transitions of one molecule will therefore probe different layers of the disk: most of the emitting region detected is near the disk surface. Detailed radiative transfer modeling indicates that LTE is not appropriate in these regions. With this two-dimensional model and the column densities from the detection of the HCO^+ and N_2H^+ ions, we derive a lower limit to the fractional ionization of 10^{-8} and an N_2/CO ratio of 2, which reveals a region where CO is heavily depleted, but N_2 is not. This zone must be well protected by the efficient shielding of ultraviolet radiation by an overlying disk layer. Additional discussions concerning the UV field, and its impact on disk chemistry will be presented in forthcoming papers.

The Owens Valley Radio Observatory is supported by NSF grant AST 99-81546. We are grateful to those OVRO staff members who diligently scheduled these time-consuming observations. We thank P. D'Alessio for providing the disk model of LkCa 15, D. Wilner and G. Sandell for sharing their unpublished data, and M. Hugerheijde for the development and use of the two-dimensional Monte Carlo radiative transfer model. J. E. K. is supported by the NASA Graduate Student Researchers Program, NGT5-50231. G.A.B. gratefully acknowledges support from the NASA Exobiology and Origins of Solar Systems programs.

REFERENCES

Aikawa, Y., & Herbst, E. 1999, ApJ, 526, 314
Aikawa, Y., Miyama, S. M., Nakano, T., & Umebayashi, T. 1996, ApJ, 467, 684
Aikawa, Y., Umebayashi, T., Nakano, T., & Miyama, S. 1998, in Faraday Discuss. 109, Chemistry and Physics of Molecules and Grains in Space, 281
———. 1999, ApJ, 519, 705
Aikawa, Y., van Zadelhoff, G. J., van Dishoeck, E. F., & Herbst, E. 2002, A&A, 386, 622
Alexander, C. M. O., Boss, A. P., & Carlson, R. W. 2001, Science, 293, 64
Amelin, Y., Krot, A., Hutcheon, I., & Ulyanov, A. 2002, Science, 297, 1678
Balbus, S. A., & Hawley, J. F. 1991, ApJ, 376, 214
Bar-Nun, A., Kleinfeld, I., & Kochavi, E. 1988, Phys. Rev. B, 38, 7749
Beckwith, S. V. W., Sargent, A. I., Chini, R. S., & Guesten, R. 1990, AJ, 99, 924
Bergin, E. A., Ciardi, D. R., Lada, C. J., Alves, J., & Lada, E. A. 2001, ApJ, 557, 209
Boogert, A. C. A., Hogerheijde, M. R., & Blake, G. A. 2002, ApJ, 568, 761
Bouvier, J., Covino, E., Kovo, O., Martin, E. L., Matthews, J. M., Terranegra, L., & Beck, S. C. 1995, A&A, 299, 89
Caselli, P., Walmsley, C. M., Zucconi, A., Tafalla, M., Dore, L., & Myers, P. C. 2002, ApJ, 565, 344
Chiang, E. I., & Goldreich, P. 1997, ApJ, 490, 368
Chiang, E. I., Joung, M. K., Creech-Eakman, M. J., Qi, C., Kessler, J. E., Blake, G. A., & van Dishoeck, E. F. 2001, ApJ, 547, 1077
Choi, M., Evans, N. J., Gregersen, E. M., & Wang, Y. 1995, ApJ, 448, 742
D'Alessio, P., Calvet, N., & Hartmann, L. 1997, ApJ, 474, 397
———. 2001, ApJ, 553, 321
Duvert, G., Guilloteau, S., Ménard, F., Simon, M., & Dutrey, A. 2000, A&A, 355, 165
Elias, J. H. 1978, ApJ, 224, 857
Feigelson, E. D., & Montmerle, T. 1999, ARA&A, 37, 363
Fromang, S., Terquem, C., & Balbus, S. A. 2002, MNRAS, 329, 18
Gammie, C. F. 1996, ApJ, 457, 355
Glassgold, A. E., Feigelson, E. D., & Montmerle, T. 2000, Protostars and Planets IV, ed. V. Mannings, A. Boss, & S. S. Russell (Tucson: Univ. Arizona Press), 429
Hayashi, C. 1981, Prog. Theor. Phys., 70, 35
Hildebrand, R. H. 1983, QJRAS, 24, 267
Hogerheijde, M. R., & van der Tak, F. F. S. 2000, A&A, 362, 697
Horne, K., & Marsh, T. R. 1986, MNRAS, 218, 761
Igea, J., & Glassgold, A. E. 1999, ApJ, 518, 848
Kastner, J. H., Zuckerman, B., Weintraub, D. A., & Forveille, T. 1997, Science, 277, 67
Kitamura, Y., Momose, M., Yokogawa, S., Kawabe, R., Tamura, M., & Ida, S. 2002, ApJ, 581, 357
Koerner, D. W. 1995, Ph.D. thesis, Caltech
Krist, J. E., et al. 1997, in AAS Meeting, 191, 0514
Lada, E. A. 1999, in NATO ASIC Proc. 540, The Origin of Stars and Planetary Systems, 441
Langer, W. D. 1985, in Protostars and Planets II, ed. D. C. Black & M. S. Matthews (Tucson: Univ. Arizona Press), 650
Lay, O. P., Carlstrom, J. E., & Hills, R. E. 1997, ApJ, 489, 917
Lutz, B. L., Womack, M., & Wagner, R. M. 1993, ApJ, 407, 402
Mannings, V., & Emerson, J. P. 1994, MNRAS, 267, 361
Mannings, V., Koerner, D. W., & Sargent, A. I. 1997, Nature, 388, 555
Millar, T. J., Farquhar, P. R. A., & Willacy, K. 1997, A&AS, 121, 139
Neuhaeuser, R., Sterzik, M. F., Schmitt, J. H. M. M., Wichmann, R., & Krautter, J. 1995, A&A, 297, 391
Owen, T. & Bar-Nun, A. 1995, Icarus, 116, 215
Pollack, J. B., Hollenbach, D., Beckwith, S. V. W., Simonelli, D. P., Roush, T., & Fang, W. 1994, ApJ, 521, 615
Robberto, M., Meyer, M. R., Natta, A., & Beckwith, S. V. W. 1999, The Universe as Seen by ISO (ESA SP-427); (Noordwijk: ESA), 195
Sargent, A. I., & Beckwith, S. 1987, ApJ, 323, 294
Scoville, N. Z., Carlstrom, J. E., Chandler, C. J., Phillips, J. A., Scott, S. L., Tilanus, R. P. J., & Wang, Z. 1993, PASP, 105, 1482
Simon, M., Dutrey, A., & Guilloteau, S. 2001, ApJ, 545, 1034
Skrutskie, M. F., Dutkevitch, D., Strom, S. E., Edwards, S., Strom, K. M., & Shure, M. A. 1990, AJ, 99, 1187

Strom, K. M., Strom, S. E., Edwards, S., Cabrit, S., & Skrutskie, M. F. 1989, AJ, 97, 1451
Thi, W. F., et al. 2001, ApJ, 561, 1074
van Zadelhoff, G.-J., Aikawa, Y., Hogerheijde, M. R., & van Dishoeck, E. F. 2003, A&A, 397, 789
van Zadelhoff, G.-J., van Dishoeck, E. F., Thi, W.-F., & Blake, G. A. 2001, A&A, 377, 566
Willacy, K., & Langer, W. D. 2000, ApJ, 544, 903
Wilner, D. J., Ho, P. T. P., & Rodriguez, L. F. 1996, ApJ, 470, L117
Womack, M., Ziurys, L. M., & Wyckoff, S. 1992, ApJ, 393, 188
Wyckoff, S., Tegler, S. C., & Engel, L. 1991, ApJ, 367, 641
Wyckoff, S. & Theobald, J. 1989, Adv. Space Res., 9, 157